Editors' Suggestion

Massive Suppression of Proximity Pairing in Topological $(Bi_{1-x}Sb_x)_2Te_3$ Films on Niobium

Joseph A. Hlevyack,[1,2,‡] Sahand Najafzadeh,[3,‡] Meng-Kai Lin,[1,2] Takahiro Hashimoto,[3] Tsubaki Nagashima,[3] Akihiro Tsuzuki,[3] Akiko Fukushima,[3] Cédric Bareille,[3] Yang Bai,[1,2] Peng Chen,[1,2,4,5] Ro-Ya Liu,[1,2,6] Yao Li,[1,2] David Flötotto,[7] José Avila,[8] James N. Eckstein,[1,2] Shik Shin,[9] Kozo Okazaki,[3,*] and T.-C. Chiang[1,2,†]

[1]*Department of Physics, University of Illinois at Urbana-Champaign, Urbana, Illinois 61801, USA*
[2]*Frederick Seitz Materials Research Laboratory, University of Illinois at Urbana-Champaign, Urbana, Illinois 61801, USA*
[3]*Institute for Solid State Physics, The University of Tokyo, Kashiwa, Chiba 277-8581, Japan*
[4]*Shanghai Center for Complex Physics, School of Physics and Astronomy, Shanghai Jiao Tong University, Shanghai 200240, China*
[5]*Key Laboratory of Artificial Structures and Quantum Control (Ministry of Education), Shenyang National Laboratory for Materials Science, School of Physics and Astronomy, Shanghai Jiao Tong University, Shanghai 200240, China*
[6]*Advanced Light Source, Lawrence Berkeley National Laboratory, Berkeley, California 94720, USA*
[7]*Center for Soft Nanoscience, University of Münster, 48149 Münster, Germany*
[8]*Synchrotron SOLEIL and Université Paris-Saclay, L'Orme des Merisiers, BP48, 91190 Saint-Aubin, France*
[9]*Office of University Professor, The University of Tokyo, Kashiwa, Chiba 277-8581, Japan*

(Received 9 March 2020; accepted 21 May 2020; published 12 June 2020)

Interfacing bulk conducting topological Bi_2Se_3 films with *s*-wave superconductors initiates strong superconducting order in the nontrivial surface states. However, bulk insulating topological $(Bi_{1-x}Sb_x)_2Te_3$ films on bulk Nb instead exhibit a giant attenuation of surface superconductivity, even for films only two layers thick. This massive suppression of proximity pairing is evidenced by ultrahigh-resolution band mappings and by contrasting quantified superconducting gaps with those of heavily *n*-doped topological Bi_2Se_3/Nb. The results underscore the limitations of using superconducting proximity effects to realize topological superconductivity in nearly intrinsic systems.

DOI: 10.1103/PhysRevLett.124.236402

Topological superconductors are among the most unconventional states of matter, wherein exotic *p*-wavelike pairing and time-reversal symmetry can foster supersymmetry and zero-energy excitations called Majorana bound states [1–7]. These emergent quasiparticles obey a non-Abelian statistics pertinent to topological quantum computing [5–7]. Despite evidence in $Cu_xBi_2Se_3$, the ruthenates, iron-based superconductors, and perhaps K-doped β-$PdBi_2$ [5–10], robust topological superconducting states remain elusive due to the often small superconducting gap and low transition temperature in candidate materials [6–9]. One promising alternative for realizing this state is to couple topological insulators (TIs) to a superconductor (SC) so that *p*-wavelike pairing is induced into the topological boundary states via the superconducting proximity effect [4–7]. Though proximity-induced superconductivity has been confirmed in the TIs Bi_2Te_3 and Bi_2Se_3 by transport [11–13], scanning tunneling spectroscopy [14–17], and momentum-resolved probe such as angle-resolved photoemission spectroscopy (ARPES) [18,19], the requirements for inducing superconductivity into the surface states are mostly unknown. Prior ARPES studies have shown proximity pairing in the nontrivial surface states of Bi_2Se_3 prepared on $NbSe_2$ and Nb [18,19], but for Bi_2Se_3 interfaced with the *d*-wave SC $Bi_2Sr_2CaCu_2O_{8+\delta}$, the proximity effect is suppressed [20,21]. Various reasons for this contrast are conjectured, including Fermi surface and/or lattice mismatch at the TI-SC interface and the short superconducting coherence length of a *d*-wave SC [20,21]. Furthermore, quantum-mechanical coupling between bulk and surface states likely drives the proximity effect in TIs-Nb, as both states exhibit the same superconducting gap in Bi_2Se_3/Nb despite different characters of the Cooper pairs [19]. Moreover, all TI-SCs containing Bi_2Te_3 and Bi_2Se_3 suffer from intrinsic bulk-carrier doping of the TI, complicating any superconductivity signatures in the surface states [14–21], and do not contain TIs in the real sense with conducting boundary states but insulating bulk.

Here, we present ultrahigh-resolution ARPES mappings of clean, bulk insulating $(Bi_{1-x}Sb_x)_2Te_3$ $(x = 0.62)$ on superconducting Nb substrate as a function of TI film thickness and temperature, which together with Bi_2Se_3/Nb reveal the pivotal role of bulk states in transiting superconductivity to the surfaces of TIs-Nb. To circumvent the inherent difficulties in growing TIs on Nb substrates [19], we employ a novel cleavage-based flip-chip method, which upon cleaving yields for the first time nearly intrinsic TI films of specific thicknesses, even in the ultrathin-film limit, on superconducting bulk Nb films. Proximity-induced superconducting gaps for slightly

n-doped $(Bi_{1-x}Sb_x)_2Te_3$/Nb are quantified and strongly contrasted with those of heavily n-doped Bi_2Se_3/Nb from our prior work, which revealed a substantial proximity-induced gap with a long decay length [19]. Our results demonstrate a massive attenuation of surface superconductivity in $(Bi_{1-x}Sb_x)_2Te_3$/Nb compared to Bi_2Se_3/Nb, suggesting that quantum-mechanical coupling between bulk and surface states largely dominates the proximity effect in TIs-Nb.

Prior to growths of $(Bi_{1-x}Sb_x)_2Te_3$ films by molecular beam epitaxy (MBE) at the University of Illinois, 6H-SiC (0001) substrates were repeatedly flash annealed to ~1300 °C to fabricate well-ordered bilayer-graphene surfaces [22]. High-purity Bi, Sb, and Te were coevaporated from an electron-beam evaporator (Bi) and effusion cells (Sb and Te) onto a substrate held at 280 °C. The film growth rate was 1 quintuple layer (QL) (1 QL ≈ 1 nm) every ~12 min; the alloy ratio $x = 0.62$ was calibrated *in situ* with a quartz crystal microbalance monitor so that the Fermi level crosses only the surface states just above the Dirac point [23]. Each $(Bi_{1-x}Sb_x)_2Te_3$ sample was post-annealed at 310 °C for ~30 min to smoothen the film further. Sample quality was confirmed *in situ* with reflection high-energy electron diffraction (RHEED) and ARPES. Ultrathin Bi_2Se_3 films were prepared on *in situ* ozone-cleaned $Al_2O_3(0001)$ substrates via a "two-step" approach [19]. Bi and Se were coevaporated onto a substrate held at 220 °C for the first two QLs and then at 280 °C for the remaining QLs; each sample was post-annealed under a lower Se flux for ~3 h at 280 °C. To prepare TIs-Nb, a 600-Å-thick polycrystalline Nb film was sputter deposited onto each TI film at ~25 °C under an Ar gas pressure of 3 mTorr and at a power of 120 W. These samples were flipped over and glued onto a polished copper sheet with low-temperature-curing Ag epoxy. A cleave pin was lastly fixed to the substrate's backside using Torr seal or Ag epoxy. Ultrahigh-resolution ARPES measurements were performed at the Institute for Solid State Physics at the University of Tokyo in a laser-based ARPES setup, which consisted of a vacuum ultraviolet laser (6.994-eV photons), a Scienta HR8000 hemispherical analyzer, and a sample manipulator cooled with superfluid liquid helium. The sample temperature was varied from 15 to 1.5 K, and the energy resolution was better than 1.5 meV. For details of the Fermi-level calibration with a gold reference, see the Supplemental Material [24] and methods in Refs. [25,26]. ARPES spectra of as-grown TIs and TI-Nb systems were taken at the University of Illinois at 18 K using a He discharge lamp. Synchrotron results were measured at the ANTARES beamline of Synchrotron SOLEIL at 80 K and an energy resolution of 15 meV.

A schematic of bulk-carrier doping in the band structure of prototypical TIs such as Bi_2Se_3 and Bi_2Te_3 is shown in Fig. 1(a), where $n+$ doping from chalcogen vacancies pins the Fermi level to the conduction band [23,27]. This carrier doping is a serious issue as the unique transport properties of Dirac fermions are obscured by trivial bulk carriers, thus complicating any signatures of the proposed Majorana bound state in TI-SC systems [21,23]. One method for isolating surface from bulk carriers is to introduce bulk Sb alloying into the parent compound Bi_2Te_3 [Fig. 1(b)] [23]. Both the Dirac point and surface states can be isolated from the conduction and valence bands by tuning the alloy ratio x in $(Bi_{1-x}Sb_x)_2Te_3$ [23,28–30]. Slightly n-doped ultrathin $(Bi_{1-x}Sb_x)_2Te_3$ films ($x = 0.62$) of thicknesses $N =$ 2–10 QLs are grown on bilayer-graphene-terminated 6H-SiC(0001) (BLG-SiC) substrates. A representative *in situ* RHEED pattern of a 2 QL film is shown in Fig. 1(c); the sharp RHEED pattern is indicative of a well-ordered film. ARPES maps and corresponding second-derivative spectra taken along $\overline{\Gamma K}$ of an as-grown 2 QL film [left and right panels of Fig. 1(d), respectively] show a distinctive but gapped Dirac cone. In the second-derivative map of Fig. 1(d), a small hybridization gap (~0.08 eV) is discernible in the Dirac cone, a quintessential feature in ultrathin TI films arising from quantum tunneling between surface states on both film boundaries [35,36]. No conduction bands are visible in these maps. Thus, these $(Bi_{1-x}Sb_x)_2Te_3$ films are bulk insulating with only the surface states crossing the Fermi level even in the ultrathin-film limit.

Figure 1(e) shows an illustration of our flip-chip method for preparing TIs on the isotropic s-wave superconductor Nb. Once $(Bi_{1-x}Sb_x)_2Te_3$/Nb ($x = 0.62$) films of thicknesses $N = 2$–10 QLs are prepared on BLG-SiC, a 600-Å-thick polycrystalline Nb film is sputter deposited onto each film at ~25 °C [step 1 in Fig. 1(e)]. These samples are flipped over [step 2 in Fig. 1(e)] and glued onto a polished copper plate using Ag epoxy with the Nb surface facing downward. Lastly, the sample structure is topped with a cleave pin [Figs. 1(e), step 3 and 1(f)]. Each sample is introduced into the ARPES system, and prior to the measurement, the sample is cleaved *in situ* by pushing sideways against the cleave pin, exposing a fresh TI surface [Fig. 1(g)]. Per prior studies on Bi_2Se_3/Nb [19] and ARPES maps in Figs. 1(h) and 1(i), the cleavage occurs exactly at the substrate-TI interface, which involves incommensurate van der Waals bonding, as the weakest point in this sample structure, resulting in a TI film of a thickness predetermined by the MBE growth on a superconducting Nb substrate.

ARPES band maps and corresponding second-derivative spectra of $(Bi_{1-x}Sb_x)_2Te_3$/Nb taken along $\overline{\Gamma M}$ and with TI film thicknesses $N = 2$–4 QLs [Figs. 1(h) and 1(i), respectively] exhibit sharp Dirac cones. No conduction bands are discernible, demonstrating that all films prepared on Nb are all n type with no bulklike states at the Fermi level. An apparent closing of the hybridization gap in the 2 QL spectra of Figs. 1(h) and 1(i) can be attributed to interactions at the TI-Nb interface, which lift the degeneracy between the topological surface states on the TI film's two boundaries, each having penetration depths of about

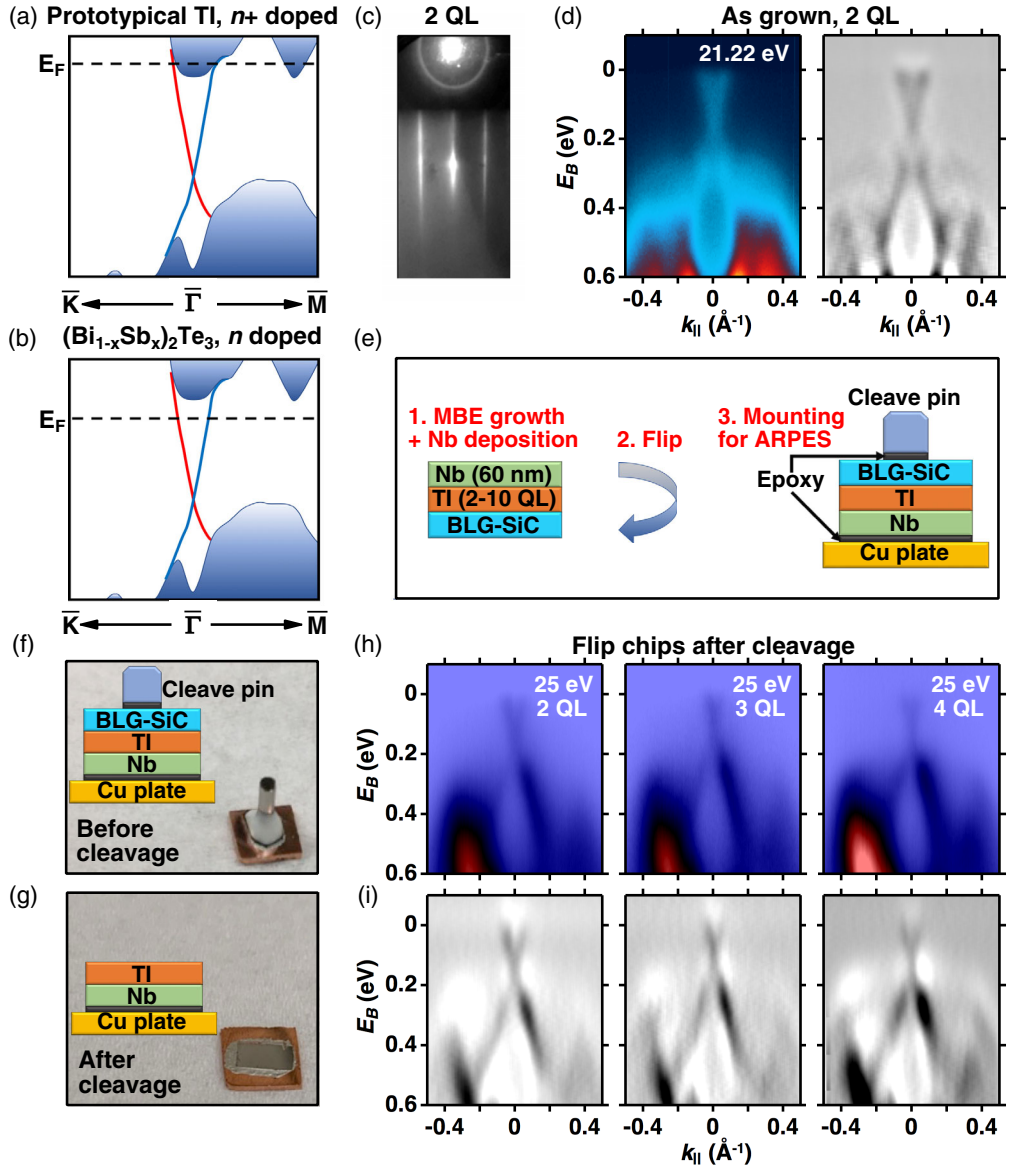

FIG. 1. Flip-chip method and characterizing lightly n-type TIs. (a),(b) Schematic band structures of n+-doped prototypical TIs and lightly n-doped $(Bi_{1-x}Sb_x)_2Te_3$, respectively. Fermi levels are indicated with black dashed lines. (c) RHEED pattern of a 2 QL $(Bi_{1-x}Sb_x)_2Te_3$ film ($x = 0.62$) grown on BLG-SiC. (d) ARPES spectra (left) and corresponding second-derivative map (right) of 2 QL $(Bi_{1-x}Sb_x)_2Te_3$ taken along $\overline{\Gamma K}$ with 21.22-eV photons at 18 K. (e) Illustration of flip-chip technique for preparing TIs on superconducting Nb substrates. (f) Photo and diagram of flip-chip sample structure before cleavage. (g) Similar as in (f) but after cleavage. (h) ARPES maps of 2–4 QL $(Bi_{1-x}Sb_x)_2Te_3$/Nb ($x = 0.62$) flip-chip samples taken with 25-eV photons at 80 K. (i) Corresponding second-derivative maps.

1 QL [35,37]. The decoupling of the surface states at the films' two boundaries well isolates those at the top surface from the substrate, even at a film thickness of just 2 QLs. These ARPES results establish a novel nearly intrinsic TI-SC system wherein the density of bulklike states at the Fermi level is fully suppressed even in the ultrathin-film limit, quite different from the TIs Bi_2Te_3 and Bi_2Se_3 prepared on a SC [14–21].

Ultrahigh-resolution ARPES band maps taken about the zone center are measured at temperatures $T = 1.5$–15 K for all samples. Example datasets for 4 QL Bi_2Se_3/Nb [19] and 4 QL $(Bi_{1-x}Sb_x)_2Te_3$/Nb are shown in Fig. 2. At $T = 10$ K, these two systems exhibit thermally broadened Fermi edges [top panels of Figs. 2(b) and 2(f)], but at $T < 2.2$ K, their behaviors diverge remarkably: 4 QL Bi_2Se_3/Nb exhibits coherence peaks, leading edge shifts, and the onset of a superconducting gap, while 4 QL $(Bi_{1-x}Sb_x)_2Te_3$/Nb shows only a sharpened Fermi edge with no identifiable coherence peak and no clear leading edge shift [bottom panels of Figs. 2(b) and 2(f),

respectively]. This sharp contrast at low temperatures is further highlighted by symmetrizing the momentum-resolved maps about the Fermi level [Figs. 2(c) and 2(g)]. To underscore the divergence between these TI-Nb systems and precisely quantify leading edge shifts, k-space integrated energy distribution curves (EDCs) and corresponding symmetrized EDCs taken as a function of temperature are summarized in Fig. 2(d) for 4 QL Bi_2Se_3/Nb and in Fig. 2(h) for 4 QL $(Bi_{1-x}Sb_x)_2Te_3$/Nb. As the sample is cooled from $T = 10$ K to $T < 2.2$ K, clear leading edge shifts and coherence peaks develop in the EDCs of 4 QL Bi_2Se_3/Nb [Fig. 2(d), top panel] but are both lacking in 4 QL $(Bi_{1-x}Sb_x)_2Te_3$/Nb [Fig. 2(h), top panel]. The symmetrized data of 4 QL Bi_2Se_3/Nb show the onset of a superconducting gap [Fig. 2(d), bottom panel], while that of 4 QL $(Bi_{1-x}Sb_x)_2Te_3$/Nb flat lines within the noise-uncertainty level at all temperatures [Fig. 2(h), bottom panel], indicating that no superconducting gap is detected at these temperatures. Thus, while 4 QL Bi_2Se_3/Nb unambiguously exhibits proximity-induced superconductivity, 4 QL $(Bi_{1-x}Sb_x)_2Te_3$/Nb shows no signs of superconductivity within the experimental energy resolution.

Because of the massive suppression of proximity-induced superconductivity in 4 QL $(Bi_{1-x}Sb_x)_2Te_3$/Nb, thickness-dependent ARPES spectra as a function of temperature are taken to reveal whether superconductivity

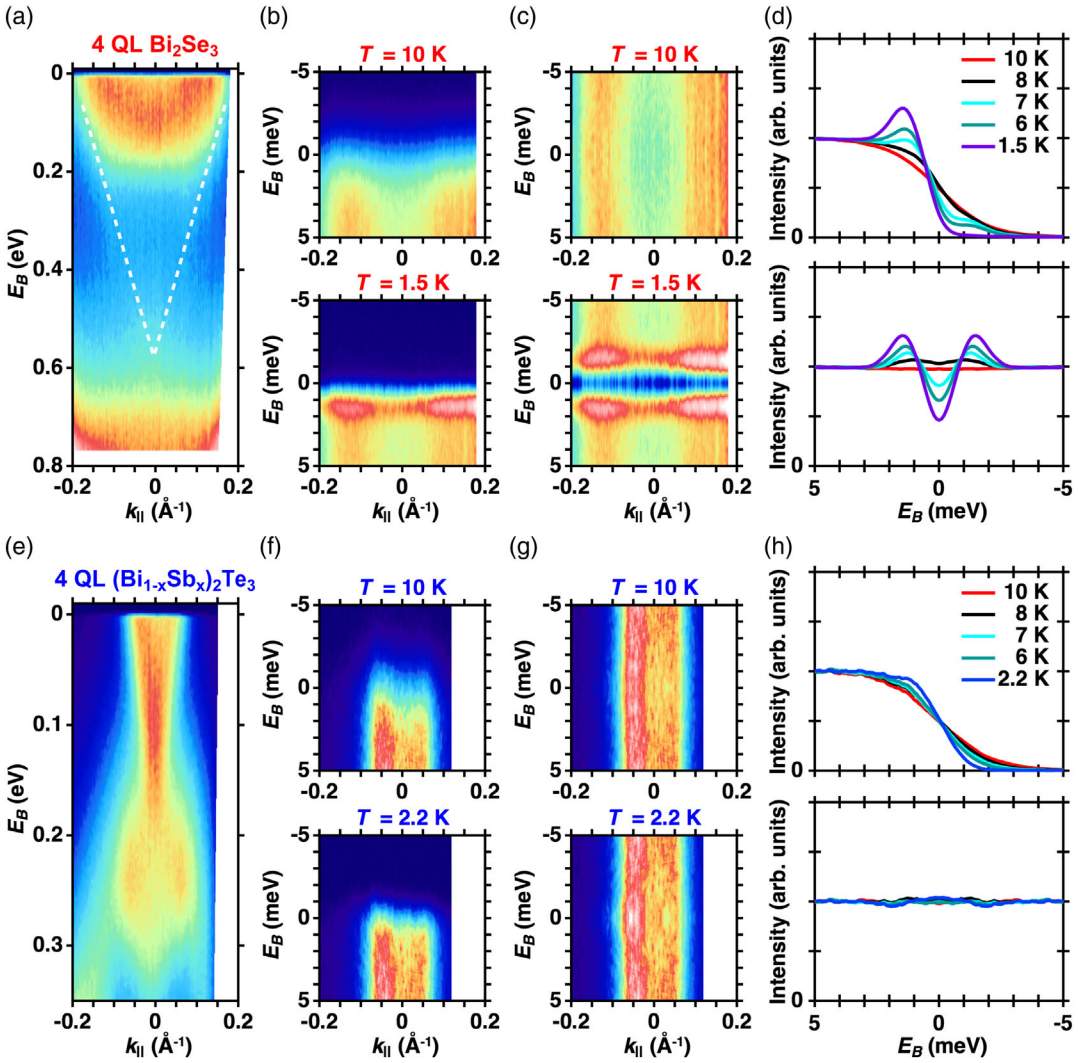

FIG. 2. Contrast between surface superconductivity in n+-doped TIs and n-type TIs. (a) ARPES map of 4 QL Bi_2Se_3/Nb taken with 6.994-eV photons at $T = 10$ K. The dashed white lines are guides to the eye that identify the Dirac cone. (b) Detailed ARPES spectra for binding energies near the Fermi level for 4 QL Bi_2Se_3/Nb at $T = 10$ K (top) and $T = 1.5$ K (bottom). (c) Corresponding symmetrized ARPES spectra, showing superconducting gaps and coherence peaks at all measured momenta at $T = 1.5$ K. (d) k-space integrated EDCs as a function of temperature (top) and corresponding symmetrized EDCs (bottom), with the k-space integration taken over the Dirac cone (from −0.18 to 0.18 Å^{-1}). (e)–(h) Corresponding dataset for 4 QL $(Bi_{1-x}Sb_x)_2Te_3$/Nb for $x = 0.62$, which reveals no superconductivity signatures; the k-space integration in (h) is taken over the Dirac cone (from −0.1 to 0.1 Å^{-1}).

can be detected in $(Bi_{1-x}Sb_x)_2Te_3$/Nb at reduced TI film thicknesses. Figure 3 displays the k-space integrated EDCs of $(Bi_{1-x}Sb_x)_2Te_3$/Nb as a function of both TI film thickness and temperature compared with Bi_2Se_3/Nb [right and left panels of Fig. 3, respectively]; Fig. 4 shows these same EDC datasets symmetrized about the Fermi level. For comparison, k-space integrated EDCs and associated symmetrized EDCs of a bare polycrystalline Nb sample are shown at the tops of Figs. 3 and 4, respectively. In all measured $(Bi_{1-x}Sb_x)_2Te_3$/Nb ($N = 2$–5 QLs), the EDCs in Fig. 3 as a function of temperature seemingly only exhibit a sharpening of the Fermi edge upon cooling from $T = 10$ K and no leading edge shift; all symmetrized EDCs in Fig. 4 thus show no development of a superconducting gap, only occasional bumps and wiggles in the EDCs at low temperatures, attributable to slight errors in Fermi-level alignment on the order of the analyzer's energy resolution (~100 μeV) [25,26]. This is in stark contrast to Bi_2Se_3/Nb [19]: Clear leading edge shifts and coherence peaks in the EDC curves in Fig. 3 arise upon cooling from $T = 10$ K for all TI film thicknesses sampled ($N = 4$–10 QLs); the symmetrized data of Bi_2Se_3/Nb in Fig. 4 show a superconducting gap for all thicknesses at the lowest temperature. Similar statements for the Nb reference are duly noted as with Bi_2Se_3/Nb. Hence, despite a clear onset of superconductivity for the Nb reference and all Bi_2Se_3/Nb ($N = 4$–10 QLs), no proximity-induced superconductivity can be observed in $(Bi_{1-x}Sb_x)_2Te_3$/Nb ($N = 2$–5 QLs).

The null results for superconductivity in $(Bi_{1-x}Sb_x)_2Te_3$/Nb are highly illuminating in regards to the coupling mechanism that may lead to topologically nontrivial superconducting pairs at surfaces. One possible cause for superconductivity at the surface of TIs-Nb is quantum-mechanical coupling between bulk and surface states [19]. Cooper pairs transferred to the Bi_2Se_3 film by Andreev reflection at the TI-SC interface reach the surface via the bulk states and/or quantum tunneling of topological interface states to the surface, though Cooper pairs lose their phase coherence with

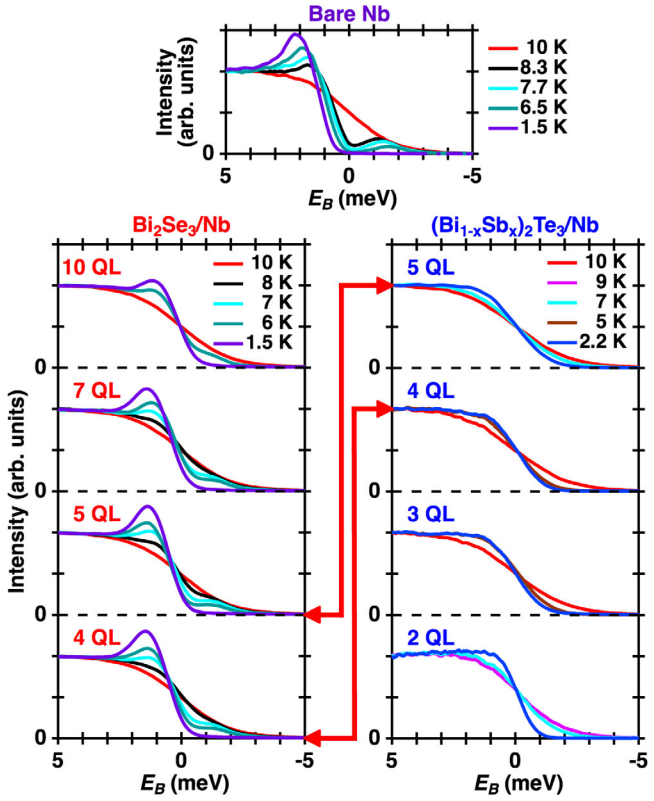

FIG. 3. k-space integrated EDCs as a function of temperature and thickness. Results are shown for a Nb reference (top), 4–10 QL Bi_2Se_3/Nb (bottom, left), and 2–5 QL $(Bi_{1-x}Sb_x)_2Te_3$/Nb for $x = 0.62$ (bottom, right). The k-space integrations are taken over −0.18 to 0.18 Å^{-1} for Bi_2Se_3/Nb and −0.1 to 0.1 Å^{-1} for $(Bi_{1-x}Sb_x)_2Te_3$/Nb. For comparisons between the measurements, the red arrows connect the spectra of 4 and 5 QL Bi_2Se_3/Nb to those of $(Bi_{1-x}Sb_x)_2Te_3$/Nb. Clear coherence peaks and leading edge shifts are visible in the Nb reference and Bi_2Se_3/Nb for all thicknesses, while none can be identified for all $(Bi_{1-x}Sb_x)_2Te_3$/Nb.

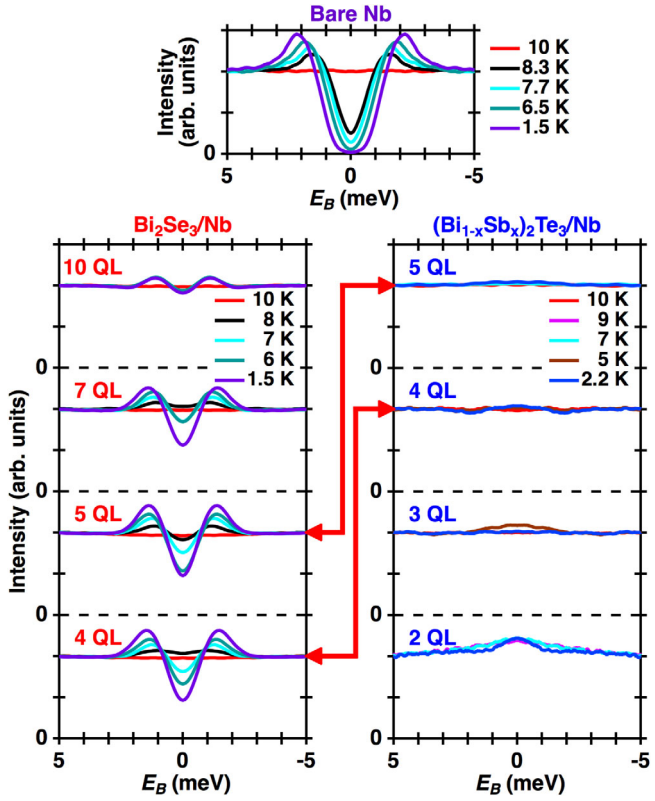

FIG. 4. Symmetrized k-space integrated EDCs as a function of temperature and film thickness. Results are summarized for a Nb reference (top), 4–10 QL Bi_2Se_3/Nb (bottom, left), and 2–5 QL $(Bi_{1-x}Sb_x)_2Te_3$/Nb for $x = 0.62$ (bottom, right). The k-space integrations are taken over −0.18 to 0.18 Å^{-1} for Bi_2Se_3/Nb and −0.1 to 0.1 Å^{-1} for $(Bi_{1-x}Sb_x)_2Te_3$/Nb. The red arrows are guides in the comparison between the datasets. As the temperature decreases from $T = 10$ K, a clear superconducting gap develops in the data of the Nb reference and all Bi_2Se_3/Nb, while none is evident for all $(Bi_{1-x}Sb_x)_2Te_3$/Nb samples.

increasing distance away from the TI-SC interface [38]. At the probed Bi_2Se_3 surface, both the topological surface and bulk states exhibit the same superconducting gap, implying that any superconducting properties impressed upon the bulk states are transferred to the surface states [19]. If there are no bulk states at the Fermi level of the TI, as in $(Bi_{1-x}Sb_x)_2Te_3/Nb$ ($x = 0.62$), then there are no bulk states or carriers that can transfer superconductivity to the topological surface states. For selenide- and telluride-based TIs, a thickness of 2 QLs is also the limit for any semblance to the bulk system, due to quantum tunneling between the topological surface states from both film boundaries [35,36]. However, since this resonant tunneling between the surface states at the two boundaries of the $(Bi_{1-x}Sb_x)_2Te_3$ films is suppressed in our case [Figs. 1(h) and 1(i)], superconducting pairing in the nontrivial boundary states at the top surface can only arise from direct coupling of these surface states to the superconducting pairs from the Nb substrate. Arguably, superconductivity at the surface may be strongly suppressed because of the very short penetration depth, about 1 QL, of the surface states [35]. The current ARPES results of Bi_2Se_3/Nb and $(Bi_{1-x}Sb_x)_2Te_3/Nb$ together support this picture, suggesting that bulk states are key for transiting superconductivity to the TI surface over any appreciable length scale. Along with employing a flip-chip technique for preparing unique TI-SC systems, our study not only unveils a mechanism for tuning the strength of the proximity effect in TIs-Nb, but also underlines the inherent limitations of using the proximity effect to realize topological superconductivity in TI-Nb systems.

This work was supported by the U.S. Department of Energy (DOE), Office of Science (OS), Office of Basic Energy Sciences, Division of Materials Science and Engineering, under Award No. DE-FG02-07ER46383 (T. C. C.), by the Ministry of Education, Culture, Sports, Science and Technology, Japan, Japan Society for the Promotion of Science KAKENHI, under Grants No. JP19H00651, No. JP19H01818, and No. JP19H05826 (K. O.), and by the Army Research Office (ARO) under Award No. W911NF-19-1-0067 (J. N. E) and the National Science Foundation (NSF) under Award No. DMR 18-36710 (J. N. E). We acknowledge that this work was partly carried out in the Central Research Facilities at the Frederick Seitz Materials Research Laboratory, University of Illinois at Urbana-Champaign; we are grateful to the staff T. Shang, F. Rao, and M. Sardela (Central Research Facilities, Frederick Seitz Materials Research Laboratory, University of Illinois at Urbana-Champaign) for providing support during the sample preparation. Synchrotron SOLEIL is supported by the Centre National de la Recherche Scientifique (CNRS) and the Commissariat à l'Energie Atomique et aux Energies Alternatives (CEA), France. This work was also supported by a public grant by the French National Research Agency (ANR) as part of the "Investissements d'Avenir" (reference: ANR-17-CE09-0016-05).

*Corresponding author.
okazaki@issp.u-tokyo.ac.jp
†Corresponding author.
tcchiang@illinois.edu
‡These authors contributed equally to this work.

[1] X.-L. Qi, T. L. Hughes, S. Raghu, and S.-C. Zhang, Phys. Rev. Lett. **102**, 187001 (2009).
[2] Z.-X. Li, Y.-F. Jiang, and H. Yao, Phys. Rev. Lett. **119**, 107202 (2017).
[3] T. Grover, D. N. Sheng, and A. Vishwanath, Science **344**, 280 (2014).
[4] L. Fu and C. L. Kane, Phys. Rev. Lett. **100**, 096407 (2008).
[5] M. Z. Hasan and C. L. Kane, Rev. Mod. Phys. **82**, 3045 (2010).
[6] M. Sato and Y. Ando, Rep. Prog. Phys. **80**, 076501 (2017).
[7] Y. Li and Z.-A. Xu, Adv. Quantum Technol. **2**, 1800112 (2019).
[8] L. A. Wray, S.-Y. Xu, Y. Xia, Y. S. Hor, D. Qian, A. V. Fedorov, H. Lin, A. Bansil, R. J. Cava, and M. Z. Hasan, Nat. Phys. **6**, 855 (2010).
[9] A. Kolapo, T. Li, P. Hosur, and J. H. Miller, Jr., Sci. Rep. **9**, 12504 (2019).
[10] P. Zhang, K. Yaji, T. Hashimoto, Y. Ota, T. Kondo, K. Okazaki, Z. Wang, J. Wen, G. D. Gu, H. Ding, and S. Shin, Science **360**, 182 (2018).
[11] B. Sacépé, J. B. Oostinga, J. Li, A. Ubaldini, N. J. G. Couto, E. Giannini, and A. F. Morpurgo, Nat. Commun. **2**, 575 (2011).
[12] J. R. Williams, A. J. Bestwick, P. Gallagher, S. S. Hong, Y. Cui, A. S. Bleich, J. G. Analytis, I. R. Fisher, and D. Goldhaber-Gordon, Phys. Rev. Lett. **109**, 056803 (2012).
[13] W. Dai, A. Richardella, R. Du, W. Zhao, X. Liu, C. X. Liu, S.-H. Huang, R. Sankar, F. Chou, N. Samarth, and Q. Li, Sci. Rep. **7**, 7631 (2017).
[14] M.-X. Wang, C. Liu, J.-P. Xu, F. Yang, L. Miao, M.-Y. Yao, C. L. Gao, C. Shen, X. Ma, X. Chen, Z.-A. Xu, Y. Liu, S.-C. Zhang, D. Qian, J.-F. Jia, and Q.-K. Xue, Science **336**, 52 (2012).
[15] J.-P. Xu, C. Liu, M.-X. Wang, J. Ge, Z.-L. Liu, X. Yang, Y. Chen, Y. Liu, Z.-A. Xu, C.-L. Gao, D. Qian, F.-C. Zhang, and J.-F. Jia, Phys. Rev. Lett. **112**, 217001 (2014).
[16] M. Chen, X. Chen, H. Yang, Z. Du, and H.-H. Wen, Sci. Adv. **4**, eaat1084 (2018).
[17] H. Zhao, B. Rachmilowitz, Z. Ren, R. Han, J. Schneeloch, R. Zhong, G. Gu, Z. Wang, and I. Zeljkovic, Phys. Rev. B **97**, 224504 (2018).
[18] S.-Y. Xu, N. Alidoust, I. Belopolski, A. Richardella, C. Liu, M. Neupane, G. Bian, S.-H. Huang, R. Sankar, C. Fang, B. Dellabetta, W. Dai, Q. Li, M. J. Gilbert, F. Chou, N. Samarth, and M. Z. Hasan, Nat. Phys. **10**, 943 (2014).
[19] D. Flötotto, Y. Ota, Y. Bai, C. Zhang, K. Okazaki, A. Tsuzuki, T. Hashimoto, J. N. Eckstein, S. Shin, and T.-C. Chiang, Sci. Adv. **4**, eaar7214 (2018).
[20] T. Yilmaz, I. Pletikosić, A. P. Weber, J. T. Sadowski, G. D. Gu, A. N. Caruso, B. Sinkovic, and T. Valla, Phys. Rev. Lett. **113**, 067003 (2014).
[21] S.-Y. Xu, C. Liu, A. Richardella, I. Belopolski, N. Alidoust, M. Neupane, G. Bian, N. Samarth, and M. Z. Hasan, Phys. Rev. B **90**, 085128 (2014).

[22] Q. Wang, W. Zhang, L. Wang, K. He, X. Ma, and Q. Xue, J. Phys. Condens. Matter **25**, 095002 (2013).
[23] J. Zhang, C.-Z. Chang, Z. Zhang, J. Wen, X. Feng, K. Li, M. Liu, K. He, L. Wang, X. Chen, Q.-K. Xue, X. Ma, and Y. Wang, Nat. Commun. **2**, 574 (2011).
[24] See Supplemental Material at http://link.aps.org/supplemental/10.1103/PhysRevLett.124.236402 for additional data and details, which includes Refs. [19,23,25–34].
[25] K. Okazaki *et al.*, Science **337**, 1314 (2012).
[26] Y. Ota, K. Okazaki, H. Q. Yamamoto, T. Yamamoto, S. Watanabe, C. Chen, M. Nagao, S. Watauchi, I. Tanaka, Y. Takano, and S. Shin, Phys. Rev. Lett. **118**, 167002 (2017).
[27] H. Zhang, C.-X. Liu, X.-L. Qi, X. Dai, Z. Fang, and S.-C. Zhang, Nat. Phys. **5**, 438 (2009).
[28] X. He, H. Li, L. Chen, and K. Wu, Sci. Rep. **5**, 8830 (2015).
[29] J. Kellner, M. Eschbach, J. Kampmeier, M. Lanius, E. Młyńczak, G. Mussler, B. Holländer, L. Plucinski, M. Liebmann, D. Grützmacher, C. M. Schneider, and M. Morgenstern, Appl. Phys. Lett. **107**, 251603 (2015).
[30] D. Hsieh, Y. Xia, D. Qian, L. Wray, F. Meier, J. H. Dil, J. Osterwalder, L. Patthey, A. V. Fedorov, H. Lin, A. Bansil, D. Grauer, Y. S. Hor, R. J. Cava, and M. Z. Hasan, Phys. Rev. Lett. **103**, 146401 (2009).
[31] I. N. Yakovkin, Crystals **6**, 143 (2016).
[32] S. M.-M. Dubois, Z. Zanolli, X. Declerck, and J.-C. Charlier, Eur. Phys. J. B **72**, 1 (2009).
[33] Y. Liu, C. Chong, W. Chen, J.-A. Huang, C. Cheng, K. Tsuei, Z. Li, H. Qiu, and V. V. Marchenkov, Jpn. J. Appl. Phys. **56**, 070311 (2017).
[34] C. Zhang, X. Yuan, K. Wang, Z.-G. Chen, B. Cao, W. Wang, Y. Liu, J. Zou, and F. Xiu, Adv. Mater. **26**, 7110 (2014).
[35] Y. Liu, G. Bian, T. Miller, M. Bissen, and T.-C. Chiang, Phys. Rev. B **85**, 195442 (2012).
[36] Y. Zhang, K. He, C.-Z. Chang, C.-L. Song, L.-L. Wang, X. Chen, J.-F. Jia, Z. Fang, X. Dai, W.-Y. Shan, S.-Q. Shen, Q. Niu, X.-L. Qi, S.-C. Zhang, X.-C. Ma, and Q.-K. Xue, Nat. Phys. **6**, 584 (2010).
[37] G. Bian, X. Wang, Y. Liu, T. Miller, and T.-C. Chiang, Phys. Rev. Lett. **108**, 176401 (2012).
[38] T. M. Klapwijk, J. Supercond. **17**, 593 (2004).